Progress in Hybrid Temporal LES (plenary lecture)

Remi Manceau

Progress in Hybrid Temporal LES

Rémi Manceau

1 Introduction

In order to favour the modelling of the subgrid stresses in continuous hybrid RANS/LES methods, the comparison of the solutions with experimental or DNS databases, and eventually the understanding of the phenomenology observed in the resolved motion, defining a rigorous formalism for such methods is highly desirable [18]. Empirical methods to bridge RANS and LES suffer from the fact that RANS and LES are based on generally inconsistent operators, statistical averaging and spatial filtering, respectively [9]. The present paper summarises recent work that tries to reconcile the two methodologies by defining consistent operators, based on temporal filtering, and provides examples of HTLES (Hybrid Temporal LES) models that can be derived based on this formalism.

2 Hybrid RANS/LES formalism

In order to build a consistent formalism for hybrid RANS/LES, it is convenient to express averaging operators, following Kampé de Fériet and Betchov [11], as the limiting case of a general spatio-temporal filtering operator

$$\widetilde{\mathbf{U}}(\mathbf{x},t) = \int_{\mathscr{D}} \int_{-\infty}^{t} G(\mathbf{x},\mathbf{x}',t,t')\mathbf{U}(\mathbf{x}',t')\,\mathrm{d}\mathbf{x}'\mathrm{d}t'. \tag{1}$$

Standard (spatial) LES is based on a filter of the form

CNRS/Univ Pau & Pays Adour,
IPRA, Department of mathematics and applied mathematics, UMR 5142,
Inria CAGIRE project team,
64000, Pau, France
remi.manceau@univ-pau.fr

$$G(\mathbf{x},\mathbf{x}',t,t') = G_S(\mathbf{x},\mathbf{x}')\delta(t-t'), \tag{2}$$

where δ denotes the Dirac delta function, parametrized by a spatial filter width Δ_S, and temporal LES (TLES [15, 16]) on

$$G(\mathbf{x},\mathbf{x}',t,t') = \delta(\mathbf{x}-\mathbf{x}')G_T(t,t'), \tag{3}$$

parametrized by a temporal filter width Δ_T.

A consistent hybrid RANS/LES formulation can be obtained if the filter kernel G goes to a low-pass filter for small filter widths and to the statistical average for infinite filter widths. In the particular case of homogeneous turbulence, statistical averaging is equivalent to spatial averaging, such that spatially filtered quantities ($\widetilde{\mathbf{U}}$) go to the statistical quantities ($\overline{\mathbf{U}}$) in the limit of an infinite filter width

$$\overline{\mathbf{U}}(t) = \lim_{\Delta_s\to\infty}\widetilde{\mathbf{U}}(\mathbf{x},t) = \lim_{\Delta_s\to\infty}\int_{\mathscr{D}}\int_{-\infty}^{t} G_S(\mathbf{x},\mathbf{x}')\delta(t-t')\mathbf{U}(\mathbf{x}',t')\,\mathrm{d}\mathbf{x}'\mathrm{d}t' \tag{4}$$

$$= \lim_{\Delta_s\to\infty}\int_{\mathscr{D}} G_S(\mathbf{x},\mathbf{x}')\mathbf{U}(\mathbf{x}',t)\,\mathrm{d}\mathbf{x}'. \tag{5}$$

Using this property, Chaouat & Schiestel [5] proposed the PITM approach, based on the equations of motion and derived from the multi-scale approach of Schiestel [17]. Although the PITM approach is developed in the framework of homogeneous turbulence, it was successfully applied to many inhomogeneous configurations (e.g., [4, 6]).

For inhomogeneous, stationary turbulence, since any temporally filtered quantity goes to the statistically averaged quantity in the limit of an infinite filter width [9], it is tempting to simplify the formalism by using a standard, Eulerian temporal filter

$$G(\mathbf{x},\mathbf{x}',t,t') = \delta(\mathbf{x}-\mathbf{x}')G_T(t,t'). \tag{6}$$

However, as shown by Speziale [19], such a filter does not satisfy Galilean invariance.

2.1 Generalized temporal filter

In order to remedy this problem, we introduce the family of generalized temporal filters

$$G(\mathbf{x},\mathbf{x}',t,t') = \delta(\xi(\mathbf{x},t,t')-\mathbf{x}')G_T(t,t'), \tag{7}$$

characterized by temporal integration at a moving application point,

$$\widetilde{\mathbf{U}}(\mathbf{x},t) = \int_{\mathscr{D}}\int_{-\infty}^{t}\delta(\xi(\mathbf{x},t,t')-\mathbf{x}')G_T(t,t')\mathbf{U}(\mathbf{x}',t')\,\mathrm{d}\mathbf{x}'\mathrm{d}t' \tag{8}$$

$$= \int_{-\infty}^{t} G_T(t,t')\mathbf{U}(\xi(\mathbf{x},t,t'),t')\,\mathrm{d}t'. \tag{9}$$

A particular case is the Lagrangian filter [13], for which $\xi(\mathbf{x},t,t') = \chi(\mathbf{x},t')$ is the fluid particle trajectory, such that

$$\widetilde{\mathbf{U}}(\mathbf{x},t) = \int_{-\infty}^{t} G_T(t,t')\mathbf{U}(\chi(\mathbf{x},t'),t')\,\mathrm{d}t'. \tag{10}$$

In order to avoid the complexity of Lagrangian filtering, while preserving Galilean invariance, a *uniform motion* of the application point is used here,

$$\xi(\mathbf{x},t,t') = \mathbf{x} + (t'-t)\mathbf{V}_{\mathrm{ref}}, \tag{11}$$

where $\mathbf{V}_{\mathrm{ref}}$ is an arbitrary velocity, constant in space and time, and the filter is referred to as the *uniform temporal filter*.

2.2 Galilean invariance

The uniform temporal filter, as the Lagrangian filter (10), is Galilean invariant. Indeed, considering a translational transformation of the reference frame defined by

$$\mathbf{x}^\star = \mathbf{x} - \mathbf{V}_0 t \tag{12}$$

where $\mathbf{x}^\star$ is the coordinate vector in the translating frame, the operator satisfies Galilean invariance if

$$\widetilde{\mathbf{U}^\star}(\mathbf{x}^\star,t) = \widetilde{\mathbf{U}}(\mathbf{x},t) - \mathbf{V}_0. \tag{13}$$

The location of the application point $\xi(\mathbf{x},t,t')$ transforms as

$$\xi^\star(\mathbf{x}^\star,t,t') = \mathbf{x}^\star + (t'-t)\mathbf{V}^\star_{\mathrm{ref}} \tag{14}$$

in the translating frame, where $\mathbf{V}^\star_{\mathrm{ref}} = \mathbf{V}_{\mathrm{ref}} - \mathbf{V}_0$. The filtered velocity then becomes

$$\begin{aligned}
\widetilde{\mathbf{U}^\star}(\mathbf{x}^\star,t) &= \int G_T(t,t')\mathbf{U}(\mathbf{x}^\star + \mathbf{V}^\star_{\mathrm{ref}}(t'-t) + t'\mathbf{V}_0, t')\,\mathrm{d}t' - \mathbf{V}_0 && (15)\\
&= \int G_T(t,t')\mathbf{U}(\mathbf{x}^\star + \mathbf{V}_0 t + (t'-t)\mathbf{V}_{\mathrm{ref}}, t')\,\mathrm{d}t' - \mathbf{V}_0 && (16)\\
&= \int G_T(t,t')\mathbf{U}(\xi(\mathbf{x},t,t), t')\,\mathrm{d}t' - \mathbf{V}_0 && (17)\\
&= \widetilde{\mathbf{U}}(\mathbf{x},t) - \mathbf{V}_0, && (18)
\end{aligned}$$

such that Galilean invariance holds.

In order to avoid any ambiguity in the definition of the filter, it is convenient to relate the velocity $\mathbf{V}_{\mathrm{ref}}$ of the application point to an element of the geometry. For instance, in a pipe flow, it is natural to choose the velocity of the pipe wall. In Fig. 1, $\mathbf{V}_{\mathrm{ref}}$ is defined as the velocity of the airplane, and the motion of the application point in two reference frames is shown. In the reference frame of the airplane (right), in

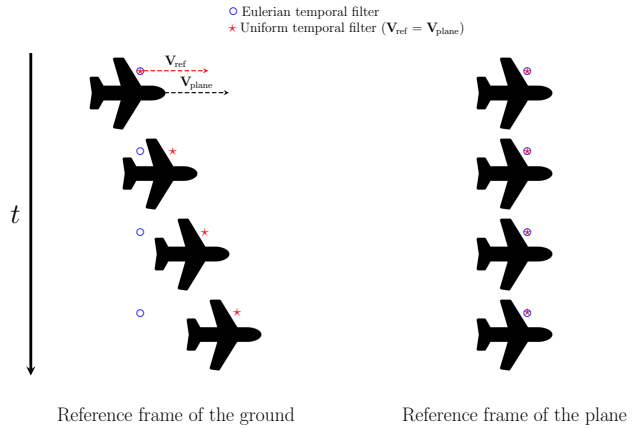

Fig. 1 Illustration of the motion of the application point of the uniform temporal filter (star), in comparison with the Eulerian temporal filter (circle), in the case of the flow around an airplane, in the reference frame of the ground (left) and of the plane (right). The reference velocity is defined as the velocity of the airplane.

which $\mathbf{V}_{\text{ref}}$ is zero, the Eulerian and uniform temporal filters are equivalent. In the reference frame of the ground (left), the application point follows the motion of the airplane, which ensures the invariance of the filter in the change of reference frame, since, at every moment, the application point corresponds to the same material point in the two reference frames. As illustrated in the figure, this is not the case for the Eulerian filter. The choice of a uniform filter with $\mathbf{V}_{\text{ref}} = \mathbf{V}_{\text{ground}}$ is legitimate (Galilean invariant), but does not meet the requirement of the hybridization of RANS and TLES, since in the reference frame of the ground, the flow is not statistically stationary, such that the filter does not go to the Reynolds average for large filter widths. A simple rule thus emerges: the reference velocity $\mathbf{V}_{\text{ref}}$ must be chosen such a way that it is zero in the reference frame in which the flow is statistically stationary. Section 4 is dedicated to the extension to fundamentally non-stationary cases, i.e., cases that are non-stationary in all the reference frames.

2.3 Consistency with long-time averaging

In the particular case of stationary turbulence, it can be easily shown that the filtered quantities go to statistically averaged quantities in the limit of infinite filter width, as illustrated in Fig. 2a, using the reference velocity $\mathbf{V}_{\text{ref}} = 0$ [10],

$$\overline{\mathbf{U}}(\mathbf{x}) = \lim_{\Delta_T \to \infty} \widetilde{\mathbf{U}}(\mathbf{x},t) = \lim_{\Delta_T \to \infty} \int_{-\infty}^{t} G_T(t,t') \mathbf{U}(\mathbf{x},t') \, \mathrm{d}t'. \tag{19}$$

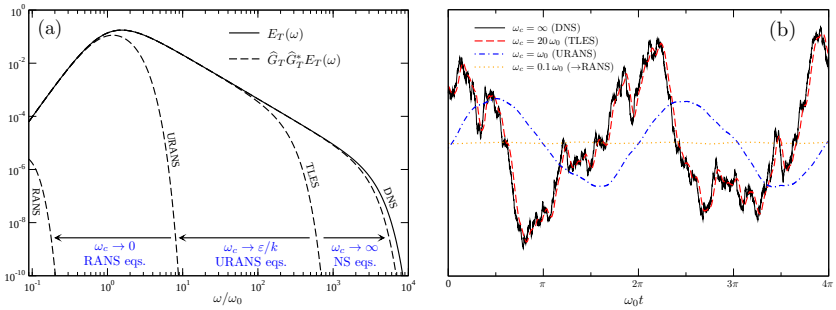

Fig. 2 (a) Generic turbulent spectrum $E_T(\omega)$ and illustration of the limiting behaviour for small and large filter widths. $\widehat{G}_T$ denotes the temporal Fourier transform of the filter and $\widehat{G}_T^*$ its complex conjugate. A Gaussian filter G_T is used here. (b) Synthetic turbulence signal as a function of time, generated using an imposed spectrum ($\omega_0 = \varepsilon/k$) and random phases. Application of a temporal filter (top-hat kernel, Fig. 6), with several cutoff frequencies ω_c.

This property is illustrated in Fig. 2b, in which a synthetic turbulent signal is generated from a generic spectrum $E_T(\omega)$ (Fig. 2a), characterized by the large-scale frequency ω_0, and random phases. A cutoff frequency of the filter in the inertial range of the spectrum defines the TLES approach. A phase shift is observed, due to the fact that the integration in Eq. (19) is performed backward in time (causal filter), i.e., is not an even function of time (see section 4.1). For very low cutoff frequencies, i.e., for temporal filter widths much larger than the integral time-scale, all the turbulent scales are filtered out and the filtered signal approaches the statistical average, which is independent of time in the present case, as seen in Fig. 2b. The intermediate case of URANS ($\omega_c \simeq \omega_0$) is investigated in section 4.1.

Assuming, as in spatial LES, that the filter commutes with the differential operators, the filtered momentum equation reads

$$\frac{\partial \widetilde{U}_i}{\partial t} + \widetilde{U}_k \frac{\partial \widetilde{U}_i}{\partial x_k} = -\frac{1}{\rho}\frac{\partial \widetilde{P}}{\partial x_i} + \nu \frac{\partial^2 \widetilde{U}_i}{\partial x_j \partial x_j} - \frac{\partial \tau_{ij_{\mathrm{sfs}}}}{\partial x_j}, \tag{20}$$

where the subfilter stress (SFS) tensor $\tau_{ij_{\mathrm{sfs}}}$ is defined as the generalized central second order moment $\tau_{ij_{\mathrm{sfs}}} = \tau(U_i, U_j)$, where $\tau(U_i,U_j) = \widetilde{U_i U_j} - \widetilde{U}_i \widetilde{U}_j$. The SFS tensor satisfies the transport equation

$$\begin{aligned}\frac{\partial \tau_{ij_{\mathrm{sfs}}}}{\partial t} + \widetilde{U}_k \frac{\partial \tau_{ij_{\mathrm{sfs}}}}{\partial x_k} = &-\frac{\partial \tau(U_i,U_j,U_k)}{\partial x_k} + \nu \frac{\partial^2 \tau_{ij_{\mathrm{sfs}}}}{\partial x_k \partial x_k} - 2\nu\,\tau\left(\frac{\partial U_i}{\partial x_k}, \frac{\partial U_j}{\partial x_k}\right) \\ &- \frac{1}{\rho}\tau\left(U_i, \frac{\partial P}{\partial x_j}\right) - \frac{1}{\rho}\tau\left(U_j, \frac{\partial P}{\partial x_i}\right) - \tau_{ik_{\mathrm{sfs}}}\frac{\partial \widetilde{U}_j}{\partial x_k} - \tau_{jk_{\mathrm{sfs}}}\frac{\partial \widetilde{U}_i}{\partial x_k},\end{aligned} \tag{21}$$

where

$$\tau(U_i,U_j,U_k) = \widetilde{U_i U_j U_k} - \widetilde{U}_i \tau(U_j,U_k) - \widetilde{U}_j \tau(U_i,U_k) - \widetilde{U}_k \tau(U_i,U_j) - \widetilde{U}_i \widetilde{U}_j \widetilde{U}_k.$$

Eq. (21) is formally identical to the familiar RANS equation for the Reynolds stress tensor $\overline{u_i u_j}$, where $u_i = U_i - \overline{U_i}$ denotes the fluctuating velocity. Moreover, as shown by Pruett *et al.* [16], the SFS tensor tends to the Reynolds-averaged tensor in the limit of infinite temporal filter width, such that the filtered equations (20) and (21) continuously go to their Reynolds averaged counterparts when the temporal filter width is gradually increased, as illustrated in Fig. 2a. This form similarity and consistency at the limit of an infinite filter width constitutes a solid foundation for developing HTLES (Hybrid Temporal LES) approaches.

3 Modelling of the subfilter stresses in HTLES

The presence of the subfilter stresses (SFS) in the equations, due to temporally filtered-out scales, lead to a closure problem similar to the case of standard LES, although the variables have a different definition. This issue was addressed in the framework of pure Temporal LES by Pruett [15], Pruett *et al.* [16] and Tejada-Martinez *et al.* [20]. For HTLES, i.e., for a cutoff frequency going to zero in some regions, as shown by Fadai-Ghotbi [7], the approach proposed by Chaouat and Schiestel [5] in the framework of spatial filtering can be transposed to uniform temporal filtering, leading to the so-called Temporal Partially Integrated Transport Method (TPITM).

3.1 Temporal PITM

The TPITM approach is based on an analysis in the frequency domain for inhomogeneous, stationary turbulence. The model is derived from the exact equation for the Eulerian temporal energy spectrum, by introducing two filters with characteristic frequencies ω_c and ω_d, as illustrated in Fig. 3a, in order to separate the resolved scales $[0;\omega_c]$, the unresolved energetic scales $[\omega_c;\omega_d]$ and the unresolved dissipative scales $[\omega_d;\infty]$. Integrating the equation for the *Eulerian temporal energy spectrum* $E_T(\mathbf{x},\omega)$ over the range $[\omega_c;\omega_d]$ (hence the name Partially Integrated Transport Model), it can be shown [7] that the modelled turbulent energy, k_m, i.e., the energy of the unresolved scales, satisfies the equation

$$\frac{Dk_m}{Dt} = P_m + D_m - \varepsilon \tag{22}$$

where P_m and D_m are the subfilter parts of the production P and the diffusion D that enter the equation for the total turbulent energy k, which is recovered term by term when $\Delta_T \to \infty$. Since one of the objectives of hybrid RANS/LES methods is not to solve the dissipative scales, ω_c must lies outside of the dissipative range, such that $\varepsilon_m = \varepsilon$. The amount of resolved energy is to be controlled by making the equations of the model dependent on the filter width, which can be achieved by

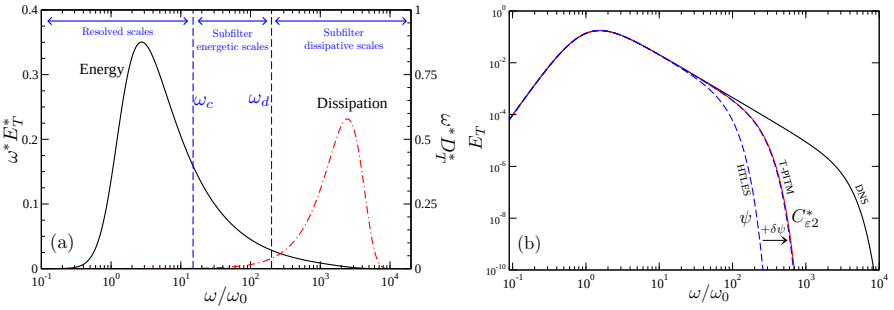

Fig. 3 (a) Definition of three spectral zones for the TPITM approach. (b) Illustration of H-equivalence. Here, the HTLES model is made H-equivalent to TPITM by introducing a variation $\delta\psi$ of the coefficient ψ.

using a transport equation for the dissipation rate that is a modification of the usual RANS equation. It can be shown [7] that the following modified dissipation rate equation can be used

$$\frac{D\varepsilon}{Dt} = C_{\varepsilon_1}\frac{\varepsilon}{k_m}P_m - C_{\varepsilon_2}^*\frac{\varepsilon^2}{k_m} + D_{\varepsilon_m}, \tag{23}$$

where D_{ε_m} is a diffusion term. The RANS/TLES transition is controlled by the variable coefficient $C_{\varepsilon_2}^* = C_{\varepsilon_1} + r\,(C_{\varepsilon_2} - C_{\varepsilon_1})$, which is a function of the ratio of modelled to total turbulent energy $r = k_{\rm sfs}/k$. The RANS limit corresponds to $r = 1$, in which case the classical RANS dissipation rate equation is recovered. Thus, TPITM is only based on a modification of the dissipation equation, which can be associated either with the transport equation for the subfilter turbulent kinetic energy $k_{\rm sfs}$ [2] (note that $k_m = \overline{k_{\rm sfs}}$) or with the transport equations for the subfilter stresses $\tau_{ij_{\rm sfs}}$ [7].

Applications of this method [7] showed the difficulty to sustain resolved turbulent fluctuations during the computation, in particular for flows that are not dominated by the Kelvin-Helmholtz instability, and the necessity of introducing a dynamic procedure to avoid a pseudo-laminarization of the computed flow. This problem can be attributed to the fact that the migration from RANS to TLES, i.e., the control of the level of subfilter energy, is only indirectly controlled via the dissipation equation. In order to address this issue, it is proposed to derive an equivalent approach, in which this control is performed via a direct modification of the dissipation term in the turbulent energy or stresses, in the spirit of DES.

3.2 A more robust Hybrid Temporal LES model

Such an approach can be obtained by defining the H-equivalence criterion, where H stands for Hybrid. Postulating that *Two hybrid approaches based on the same closure, but using a different method of control of the energy partition, yield similar*

low-order statistics of the resolved velocity fields provided that they yield the same level of subfilter energy [8], two approaches are said H-equivalent if they lead to the same partition of energy for a particular situation and tend to the same RANS model for large filter widths.

Using a perturbation method, i.e., based on infinitesimal modifications of the system of equations, it can be shown [8] that the approach based on an equation of the form

$$\frac{\mathrm{d}k_{\mathrm{sfs}}}{\mathrm{d}t} = P_{\mathrm{sfs}} - \frac{k_{\mathrm{sfs}}}{T} + D_{\mathrm{sfs}}, \tag{24}$$

simply called herafter Hybrid Temporal LES (HTLES), can be H-equivalent to the TPITM model. In order to identify the time scale T to use in Eq. (24), one can compare the behaviour of two systems of equations written for the *Reynolds-averaged* subfilter energy k_m and its dissipation rate ($k_m = \overline{k_{\mathrm{sfs}}}$): the TPITM system (25) and the HTLES system (26),

$$\begin{cases} \dfrac{\mathrm{d}k_m}{\mathrm{d}t} = P_m - \varepsilon + D_m \\ \dfrac{\mathrm{d}\varepsilon}{\mathrm{d}t} = C_{\varepsilon 1}\dfrac{\varepsilon}{k_m}P_m - C^*_{\varepsilon 2}\dfrac{\varepsilon^2}{k_m} - D_\varepsilon \end{cases} \tag{25}$$

$$\begin{cases} \dfrac{\mathrm{d}k_m}{\mathrm{d}t} = P_m - \psi\,\varepsilon + D_m \\ \dfrac{\mathrm{d}\varepsilon}{\mathrm{d}t} = C_{\varepsilon 1}\dfrac{\varepsilon}{k_m}P_m - C_{\varepsilon 2}\dfrac{\varepsilon^2}{k_m} - D_\varepsilon \end{cases} \tag{26}$$

where $\psi = k_m/(\varepsilon T)$. Ensuring H-equivalence between the two systems of equations raises the question: *How must the ψ function be chosen for the HTLES system Eq. (26) to provide the same level of modelled energy k_m as the TPITM system Eq. (25)?* H-equivalence, applied to HTLES and TPITM, is illustrated in Fig. 3b: a computation using this HTLES model reproduces a filtered spectrum, with a cutoff frequency depending on the coefficient ψ. If this coefficient is arbitrary, there is no reason for HTLES to exhibit the same level of modelled energy (or in other words, the same partition of energy), as the TPITM. However, a modification $\delta\psi$ of the coefficient ψ can be introduced in order to drive the partition of energy toward that of the TPITM, i.e., to make HTLES H-equivalent to TPITM. The analysis below then aims at identifying the relation between the ψ and $C^*_{\varepsilon 2}$ coefficients to ensure H-equivalence.

At the RANS limit, since the prerequisite to the analysis is that the two approaches are based on the same closure, i.e., the two systems Eq. (25) and Eq. (26) go to the equations of one and the same RANS model as ω_c goes to zero, the two approaches yield the same level of subfilter energy $k_m = k$. Now, the H-equivalence of the systems can be preserved by introducing infinitesimal variations $\delta C^*_{\varepsilon 2}$ and $\delta\psi$ of the coefficients $C^*_{\varepsilon 2}$ and ψ, respectively. The two systems remain H-equivalent if the modification of the two coefficients leads to the same infinitesimal variation δk_m of the subfilter energy k_m. In some particular situations, the relation between the coefficients can be analytically obtained. The less restrictive situation is the case of inhomogeneous turbulence in straight duct flows, in which it can be shown that the two systems yield the same δk_m if

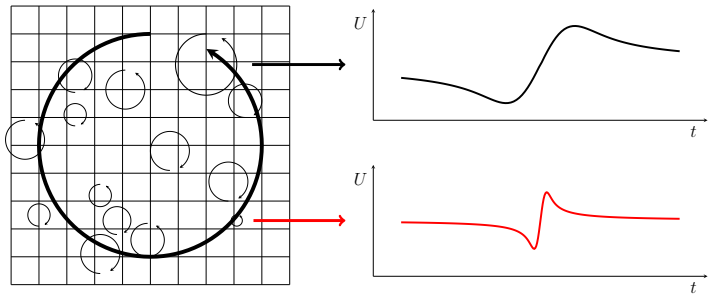

Fig. 4 Illustration of the sweeping mechanism [21] and its link with the cutoff frequency.

$$\frac{\delta\psi}{(C_{\varepsilon 2}-C_{\varepsilon 1}\psi)} = -\frac{\delta C^*_{\varepsilon 2}}{C_{\varepsilon 2}\left(C^*_{\varepsilon 2}-C_{\varepsilon 1}\right)}, \tag{27}$$

Integrating this relation from the RANS state ($C^*_{\varepsilon 2} = C_{\varepsilon 2}$ and $\psi = 1$) to an arbitrary LES state ($C^*_{\varepsilon 2} < C_{\varepsilon 2}$ and $\psi > 1$) leads to

$$\psi = 1 + \left(\frac{C_{\varepsilon 2}}{C_{\varepsilon 1}} - 1\right)\left(1 - r^{C_{\varepsilon 1}/C_{\varepsilon 2}}\right). \tag{28}$$

The conclusion of this analysis is that HTLES in equivalent to TPITM if the time scale in Eq. (24) writes

$$T = \frac{r}{1 + \left(\frac{C_{\varepsilon 2}}{C_{\varepsilon 1}} - 1\right)\left(1 - r^{C_{\varepsilon 1}/C_{\varepsilon 2}}\right)}\frac{k}{\varepsilon}. \tag{29}$$

The transport equation for k_{sfs} and ε in HTLES are formally identical to the standard RANS model equations. The modified time scale enforces the LES mode for $r < 1$ by increasing the dissipation term k_{sfs}/T in the k_{sfs}-equation, similar to two-equation DES. This method can be easily adapted to second moment closures, i.e., models based on transport equations for the subfilter stress tensor, by replacing ε in the dissipation tensor by k_{sfs}/T.

This version of Hybrid Temporal LES bears similarities with DES, but also significant differences: it is based on a modified time-scale rather than a length scale; the modification is based on the comparison of averaged quantities (r and k/ε), rather that time-dependent, filtered quantities; DES is an empirical approach, without an explicit reference to a particular formalism for bridging LES and RANS, although it can be interpreted as a simplified version of a method H-equivalent to the TPITM. The interested reader is referred to Friess *et al.* [8] for further details.

Moreover, an interesting feature is that HTLES does not explicitly involve the width of the filter, but only the ratio r that characterizes the partition of energy. It is thus possible to implement it as a purely adaptive approach, which identifies the local resolution and consequently adapts the time scale T by monitoring, during the computation, the ratio of modelled to total turbulent energy.

Another possibility is to explicitly relate the model to the filter, by modelling the ratio r as a function of the cutoff frequency ω_c. Similar to the case of the spatial filter width in LES, it appears optimal to relate the cutoff frequency to the Nyquist frequency linked to the time step dt,

$$\omega_c = \frac{2\pi}{2dt}, \tag{30}$$

such that the temporal filter width is $\Delta_T = 2dt$. However, for a sufficiently small time step, the highest frequency π/dt cannot be observed in the computation, since the corresponding eddies are filtered out by the grid, the maximum observable wavenumber being $\kappa_c = 2\pi/2\Delta$. The maximum frequency observed at a fixed point is not linked to the turnover time of the eddies of wavenumber κ_c (Lagrangian time scale), but rather to the advection (sweeping) of the small scales by the large scales [21], as illustrated in Fig. 4. The medium eddy at the top is swept by the large scale structure, such that it generates the time-dependent signal shown in the top-right figure, which can be measured, for instance, by a hot wire at a fixed point. The small eddy at the bottom would generate a signal contributing to higher frequencies if it was resolved, but since the grid is too coarse, the corresponding frequencies are missing. Therefore, the maximum observable frequency is

$$\omega_c = \min\left(\frac{\pi}{dt}; \frac{U_s\pi}{\Delta}\right), \tag{31}$$

where U_s denotes the sweeping velocity. In the absence of a mean velocity, following Tennekes [21], the sweeping velocity can be related to the characteristic velocity of the energetic eddies, $U_s = u = \gamma\sqrt{k}$, where γ is a coefficient. In the presence of a mean flow, the maximum observable frequency is related to the sweeping velocity $U_s = U + u$, with U the mean velocity magnitude.

The value of the ratio r can be related to the cutoff frequency of the temporal filter ω_c using the assumption of an equilibrium Eulerian spectrum [21], derived from the Kolmogorov wavenumber spectrum using the dispersion relation $\mathrm{d}\omega = U_s\mathrm{d}\kappa$,

$$E_T(\omega) = C_\kappa \varepsilon^{2/3} U_s^{2/3} \omega^{-5/3} \tag{32}$$

The ratio r, defined as k_m/k, can then be evaluated as

$$r = \frac{k_m}{k} = \frac{1}{k}\int_{\omega_c}^{\infty} E_T(\omega)\,\mathrm{d}\omega = \frac{3C_\kappa}{2}\left(\frac{U_s}{\sqrt{k}}\right)^{2/3}\left(\omega_c\frac{k}{\varepsilon}\right)^{-2/3}, \tag{33}$$

such that the following relation is used

$$r = \min\left(1; \frac{1}{\beta}\left(\frac{U_s}{\sqrt{k}}\right)^{2/3}\left(\omega_c\frac{k}{\varepsilon}\right)^{-2/3}\right). \tag{34}$$

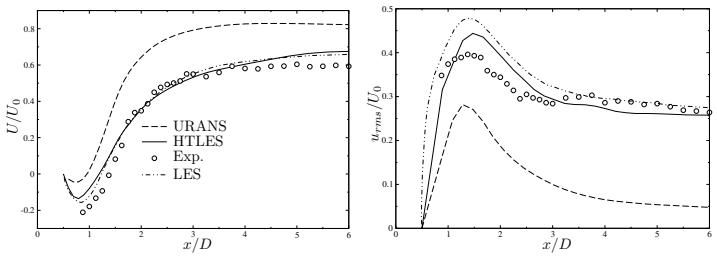

Fig. 5 HTLES computation of the flow around a square cylinder at $Re = 21400$ [22]. Mean (left) and rms (right) streamwise velocities along the axis of symmetry in the wake of the cylinder. Comparison with experiments [12], LES [3] and URANS using the same closure (k-ω-SST).

Tran *et al.* [22] used the case of homogeneous isotropic turbulence to calibrate the value of the coefficient, and obtained $\beta = 0.67$. The HTLES approach is applied here to the k-ω-SST model [14].

In order to illustrate the predictive capabilities of the method, the case of the flow around a square-sectioned cylinder in chosen, in comparison with the experimental data of Lyn *et al.* [12], for $Re = 21400$ and the recent LES of Cao and Tamura [3]. The present results are obtained using a multi-block, structured grid of about 0.5×10^6 cells (to be compared to 72.9×10^6 for the LES), with $y^+ \simeq 1$ ensured at the wall, and the spanwise extent of the domain is $4D$. Computations are performed using the open-source CFD software *Code_Saturne* [1].

Fig. 5 shows profiles extracted along the symmetry line behind the cylinder. URANS results, based on the same closure, the k-ω-SST model, obtained with the same grid, are plotted for comparison. Fig. 5 clearly shows the interest of HTLES compared to URANS, i.e., to the resolution of finer turbulent structures. Indeed, URANS severely underestimates the turbulent energy in the wake and overestimates the mean velocity. The recirculation region is predicted far too short and intensity of the backflow is strongly underestimated. With HTLES, using the same closure for the unresolved stresses, but reducing the level of modelled energy, i.e., making possible the resolution of a wider range of turbulent structures, the reproduction of this flow is drastically improved. Moreover, it is worth pointing out that HTLES results are close to LES results, although the number of cells is reduced by a factor of 145, because the near-wall region is solved in URANS mode (see section 4).

4 Non-stationary turbulence: hybrid URANS/TLES

4.1 URANS as a temporally filtered approach

URANS suffers from a lack of clear definition in general situations. For instance, in the case of stationary turbulence with coherent, quasi-periodic vortex shedding, such as the case of the wake of a stationary cylinder, with a constant inlet velocity,

as shown in section 3.2, statistically averaged quantities are independent of time, such that the temporal derivative does not appear in the RANS equations. Therefore, solving time-dependent equations with a standard RANS turbulence model appears somehow arbitrary.

However, it is interesting to note that, for coarse resolutions (large values of r), the denominator in Eq. (29) goes to unity, such that the time scale T is asymptotically equivalent to $rk/\varepsilon = k_m/\varepsilon$. In this case, the dissipation term $\psi\varepsilon = k_m/T$ in Eq. (26) is equal to ε. Similarly, in the equation (24) for $k_{\rm sfs}$, which is resolved in practice, the dissipation term $k_{\rm sfs}/T$ is equal to $(k_{\rm sfs}/k_m)\,\varepsilon$. Since $k_m = \overline{k_{\rm sfs}}$, the ratio in brackets just fluctuates around unity. The HTLES equations thus approach the URANS equations (i.e., including the time derivative, in both the turbulent energy and dissipation equations). Now, large values of r are obtained for cutoff frequencies going to $\omega_0 = U_s\kappa_0$, i.e., to the characteristic frequency corresponding to the integral scale of turbulence. Therefore, URANS can be regarded as a temporally-filtered approach in which the temporal filter width is of the order of magnitude of the eddy-turnover time of the energetic structures of the flow: $\Delta_T \simeq k/\varepsilon$, as illustrated in Fig. 2a. In flows dominated by vortex shedding, such as the flow around a square cylinder presented above, the large, coherent structures, whose time scale correspond to k/ε, i.e., to the temporal filter width, are not completely filtered-out and the resolved flow is unsteady and mostly 2D. However, since the effective filter due to the model for the subfilter stresses is not a cutoff filter but rather a filter with a transfer function less than unity for these frequencies, the amplitude of the coherent structures is reduced.

This remark can be simply illustrated by analysing the effect of the application of a temporal filter on a monochromatic wave of the form $V(x,t) = V_0\cos(k_0x - \omega_0 t)$, which can be regarded as a very simplified model for the crosswise velocity signal in, e.g., a the cylinder wake. It can be easily shown that the application, for instance, of the causal top-hat filter represented in Fig. 6 leads to a monochromatic wave with an amplitude reduced by a factor a and with a phase shift φ given by

$$a = \frac{\sin(\frac{\omega_0\Delta_T}{2})}{\frac{\omega_0\Delta_T}{2}} \quad ; \qquad \varphi = \frac{\omega_0\Delta_T}{2}. \tag{35}$$

If ω_c is the frequency ω_0 of the unfiltered wave, then the amplitude reduction and the phase shift are $2/\pi \simeq 0.63$ and $\pi/2$, respectively, as illustrated in Fig. 6. The application of such a filter with $\omega_c = \omega_0$ to a synthetic turbulent signal is shown in Fig. 2b. The filtered signal is close to periodic and monochromatic. The amplitude reduction and the phase shift clearly appear.

This interpretation of URANS as a temporally filtered approach is supported by the results shown in Fig. 5: the vortex shedding is reproduced with the correct Strouhal number (temporal filtering does not affect the frequencies); the rms velocity is severely underestimated (temporal filtering damps the amplitudes); since eddies with characteristic time scales smaller than the integral time scale are filtered out, the coherent structures are not destabilized by the nonlinear interactions with smaller scales and the resolved motion is quasi-2D and quasi-periodic.

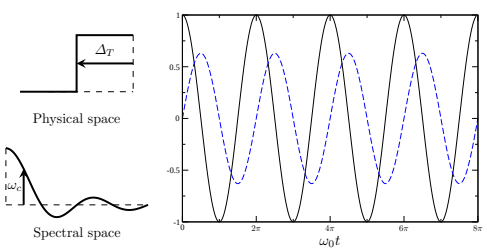

Fig. 6 Illustration of the effect of a temporal top-hat filter (left) on a monochromatic wave (right), for the particular case of a cutoff frequency ω_c equal to the frequency ω_0 of the wave: comparison of the unfiltered function $V(0,t)$ (solid line) and the filtered function $\widetilde{V}(0,t)$ (dashed line).

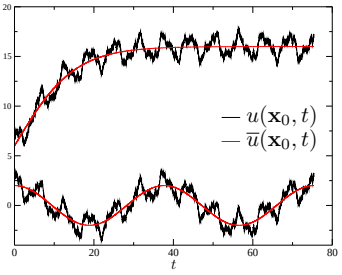

Fig. 7 Illustration of non-stationary turbulent signals: transient flow (top); cyclostationary flow (bottom).

4.2 Hybridization of TLES and URANS

URANS can be applied in practise in many different configurations, with fundamental distinctions:

- ✓ Stationary turbulence (boundary condition independent of time) dominated by large-scale, coherent structures, such as the flow around a cylinder shown in section 3.2. In this case, RANS equations are independent of time, since the statistical average is equivalent to the long-time average. As shown above, URANS equations can be obtained as the limit of HTLES equations using the integral time scale as the filter width.
- ✓ Non-stationary turbulence (statistics dependent of time). This is the case for transient flows, see Fig. 7 (top), as, e.g., the deployment of high-lift devices, in which case the RANS equations are dependent of time, and are alternatively termed as URANS (Unsteady) or TRANS (Transient). This is also the case for periodic flows (cyclostationary), see Fig. 7 (bottom), i.e., turbulent flows with an imposed periodic component, due to periodic boundary conditions (e.g., car engine, flapping wing, pulsed flow). In this case, URANS equations can be rigorously derived using phase-averaging. In both cases (transient or periodic turbulent flows), the URANS equations are also formally identical to HTLES equations with a filter width equal to the integral time scale.

Therefore, the HTLES methodology can be used to bridge URANS and TLES methods. If the grid and time steps are sufficiently fine compared to the integral length and time scales, respectively, the TLES approach is active, i.e., the cutoff frequency lies in the inertial region of the spectrum and a large portion of the energetic eddies is resolved. If the grid and/or time steps are comparable to the integral scales, the URANS approach is active. In the case of stationary turbulence, or, if the permanent state of a transient flow is reached, the URANS equations become independent of time, and HTLES reverts to the hybrid RANS/TLES approach described in section 3.

These properties of formal similarity of HTLES and URANS equations thus make possible the extension of the HTLES approach to any type of flow configurations.

5 Conclusion

Uniform temporal filtering provides a consistent formalism for hybridizing RANS and LES, or, more accurately, unsteady RANS and temporal LES. Indeed, the filtered quantities, as well as their moments, in particular the subfilter stresses, continuously go from low-pass-filtered quantities to Reynolds-averaged quantities when the temporal filter width is gradually increased. The formal similarity of the TLES and URANS equations constitutes a solid basis for the development of models for the subfilter stresses that bridge the two approaches, and ensures the validity of the approach in general configurations.

Given a formal closure of the filtered equations, either a constitutive relation for first moment closures or modelled transport equations for the subfilter stresses, the hybrid approach must be able to control the partition of energy among resolved and modelled scales. Based on the equations of motion and a partition of the energy spectrum into resolved, unresolved energetic and unresolved dissipative scales, the TPITM approach, the temporal version of the PITM, can be derived, in which the partition of energy is controlled via a variable coefficient in the dissipation equation.

In order to circumvent some difficulties faced when applying the TPITM model, a more robust HTLES approach is proposed, in which the energy partition is directly controlled by modifying the dissipation term in the energy or subfilter stress equation. If this modification is carefully designed in order to satisfy an equivalence criterion, this HTLES model preserves the good properties of TPITM, but is significantly easier to implement. This approach bears some similarities with DES, but accounts for the influence of the filter width on the equations in a very different manner.

6 Acknowledgements

Several colleagues and students have contributed over the years to the progress of temporally filtered hybrid RANS/LES approaches. They are listed alphabetically: J. Borée, A. Fadai-Ghotbi, Ch. Friess, T.B. Gatski, R. Perrin, T.T. Tran. This work was granted access to the HPC resources of IDRIS under Grant No. 2010-020912 made by GENCI (Grand Equipement National de Calcul Intensif) and to the computing facilities of the MCIA (Mésocentre de Calcul Intensif Aquitain) of the University of Bordeaux and of the University of Pau.

References

1. F. Archambeau, N. Méchitoua, and M. Sakiz. Code Saturne: A Finite Volume Code for the Computation of Turbulent Incompressible flows - Industrial Applications. *Int. J. on Finite Volume, Electronical edition: http://averoes.math.univ-paris13.fr/html*, ISSN 1634(0655), 2004.
2. Y. Bentaleb and R. Manceau. A hybrid Temporal LES/RANS formulation based on a two-equation subfilter model. In *Proc. 7th Int. Symp. Turb. Shear Flow Phenomena, Ottawa, Canada*, 2011.
3. Y. Cao and T. Tamura. Large-eddy simulations of flow past a square cylinder using structured and unstructured grids. *Comput. Fluids*, 137:36–54, 2016.
4. B. Chaouat. Subfilter-scale transport model for hybrid RANS/LES simulations applied to a complex bounded flow. *J. Turbul.*, 11(51):1–30, 2010.
5. B. Chaouat and R. Schiestel. A new partially integrated transport model for subgrid-scale stresses and dissipation rate for turbulent developing flows. *Phys. Fluids*, 17(065106):1–19, 2005.
6. A. Fadai-Ghotbi, Ch. Friess, R. Manceau, and J. Borée. A seamless hybrid RANS-LES model based on transport equations for the subgrid stresses and elliptic blending. *Phys. Fluids*, 22(055104), 2010.
7. A. Fadai-Ghotbi, Ch. Friess, R. Manceau, T.B. Gatski, and J. Borée. Temporal filtering: a consistent formalism for seamless hybrid RANS-LES modeling in inhomogeneous turbulence. *Int. J. Heat Fluid Fl.*, 31(3):378–389, 2010.
8. Ch. Friess, R. Manceau, and T.B. Gatski. Toward an equivalence criterion for hybrid RANS/LES methods. *Comput. Fluids*, 122:233–246, 2015.
9. T. B. Gatski, C. L. Rumsey, and R. Manceau. Current Trends in Modeling Research for Turbulent Aerodynamic Flows. *Phil. Trans. R. Soc. A*, 365(1859):2389–2418, 2007.
10. J. Kampé de Fériet. La notion de moyenne dans la théorie de la turbulence. In *Rendiconti del seminario matematico dell'universita e del politecnico*, pages 167–207, 1957.
11. J. Kampé de Fériet and R. Betchov. Theoretical and experimental averages of turbulent functions. *Proc. K. Ned. Akad. Wet.*, 53:389–398, 1951.
12. D.A. Lyn, S. Einav, W. Rodi, and J.-H. Park. Laser-Doppler velocimetry study of ensemble-averaged characteristics of the turbulent near wake of a square cylinder. *J. Fluid Mech.*, 304:285–319, 1995.
13. C. Meneveau, T.S. Lund, and W.H. Cabot. A Lagrangian dynamic subgrid-scale model of turbulence. *J. Fluid Mech.*, 319:353–385, 1996.
14. F. R. Menter. Two-equation eddy-viscosity turbulence models for engineering applications. *AIAA J.*, 32(8):1598–1605, 1994.
15. C. D. Pruett. Eulerian time-domain filtering for spatial large-eddy simulation. *AIAA J.*, 38(9):1634–1642, 2000.
16. C. D. Pruett, T. B. Gatski, C. E. Grosch, and W. D. Thacker. The temporally filtered Navier-Stokes equations: Properties of the residual stress. *Phys. Fluids*, 15(8):2127–2140, 2003.
17. R. Schiestel. Multiple-time-scale modeling of turbulent flows in one-point closures. *Phys. Fluids*, 30(3):722–731, 1987.
18. P.R. Spalart. Detached-eddy simulation. *Annu. Rev. Fluid Mech.*, 41:181–202, 2009.
19. C. G. Speziale. On the decomposition of turbulent flow fields for the analysis of coherent structures. *Acta Mechanica*, 70(1-4):243–250, 1987.
20. A. E. Tejada-Martinez, C. E. Grosch, and T. B. Gatski. Temporal Large eddy simulation of unstratified and stably stratified turbulent channel flows. *Int. J. Heat Fluid Fl.*, 28:1244–1261, 2007.
21. H. Tennekes. Eulerian and Lagrangian time microscales in isotropic turbulence. *J. Fluid Mech.*, 67:561–567, 1975.
22. T.T. Tran, R. Manceau, R. Perrin, J. Borée, and A.T. Nguyen. A hybrid temporal LES approach. Application to flows around rectangular cylinders. In *Proc. 9th ERCOFTAC Int. Symp. on Eng. Turb. Modelling and Measurements, Thessaloniki, Greece*, 2012.